JOURNAL OF GEOPHYSICAL RESEARCH, VOL. 113, E08014, doi:10.1029/2007JE003055, 2008

Distribution of the ices exposed near the south pole of Mars using Thermal Emission Imaging System (THEMIS) temperature measurements

Sylvain Piqueux,[1] Christopher S. Edwards,[1] and Philip R. Christensen[1]

Received 7 December 2007; revised 21 February 2008; accepted 7 April 2008; published 22 August 2008.

[1] Understanding the present and past water cycle on Mars requires an accurate knowledge of the distribution and amount of H_2O available near the surface. In this article, we present a map of the distribution of the surface material exposed between 87°S and 70°S in the summer (e.g., CO_2 and H_2O ices, dust) based on temperature measurements made by Thermal Emission Imaging System (THEMIS). Our compositional map (100 m per pixel) is in good agreement with spectral mapping returned by Observatoire pour la minéralogie, l'Eau, la Glace et l'activité (OMEGA) and Compact Reconnaissance Imaging Spectrometer for Mars (CRISM). Exposed water ice covers a total surface area of approximately 40,000 km^2. A large fraction of the water ice is exposed at the periphery of the CO_2 cap. An approximately 25,000-km^2 large patch centered at 83.5°S and 345°E is discovered and represents the largest exposure of water ice in the southern hemisphere. It is not located on the south polar layered deposits but on the surrounding mantled terrains. THEMIS VIS, MOC and HiRISE images indicate that the surface roughness of exposed water ice terrains is typically lower than that of the surrounding dust. Polygonal patterns are observed on the water ice but not exclusively. There is a strong correlation between the surface albedo, the composition of the exposed material, and the timing of the initial seasonal CO_2 frost deposition and final removal. These exposed water ice outcrops are not stable in the present environment and lose a vertical layer of tens to hundreds of micrometer a year to the atmosphere. The spike of water vapor above the south pole during the southern summer occurs while the water ice is still covered by a layer of seasonal CO_2 frost, indicating that the sublimation of the exposed water ice is not the main contributor of vapor for the southern atmosphere. As water ice is not stable, it may indicate the past location of part of the CO_2 perennial cap that has been eroded.

Citation: Piqueux, S., C. S. Edwards, and P. R. Christensen (2008), Distribution of the ices exposed near the south pole of Mars using Thermal Emission Imaging System (THEMIS) temperature measurements, *J. Geophys. Res.*, *113*, E08014, doi:10.1029/2007JE003055.

1. Introduction

[2] The south polar layered deposits (SPLD) of Mars and the surrounding mantled terrains are of high interest because they contain the largest body of water ice near the surface of Mars [*Zuber et al.*, 2007a], they have recorded the past climate and global catastrophic events modifying the surface [*Clifford et al.*, 2000], and because they concentrate some of the most dynamic processes shaping the surface within a single region. These dynamic processes include the waning and waxing of the seasonal cap, basal sublimation and venting of the seasonal CO_2 frost leading to the formation of spiders and etched polygons [*Kieffer et al.*, 2006; *Kieffer*, 2007; *Piqueux and Christensen*, 2008b], expansion and contraction of the perennial cap over many years [*Piqueux and Christensen*, 2008a], possible initiation of local dust storms due to high atmospheric thermal gradients [*Toigo et al.*, 2002 and references therein], and trapping and release of volatiles in the atmosphere during climate shifts [*Ingersoll*, 1974; *Toon et al.*, 1980; *Fanale and Jakosky*, 1982; *Jakosky and Carr*, 1985; *Mellon and Jakosky*, 1995; *Mellon et al.*, 2004]. The ices exposed at the surface form the interface between the solid water and the atmospheric reservoirs. The details of the exchange of volatiles between these two reservoirs must be well constrained to understand the current and past climates of Mars. This article contributes to this effort by presenting a thermal analysis of the near surface of the SPLD using the Mars Odyssey Thermal Emission Imaging System (THEMIS), allowing us to map the distribution of the surface materials,

[1]School of Earth and Space Exploration, Arizona State University, Tempe, Arizona, USA.

0148-0227/08/2007JE003055$09.00

namely CO_2 and H_2O ices and particulated material (dust and sand).

2. Background

[3] Several instruments, beginning with the Mariner 9 cameras in the 1970s, have provided albedo, morphological, thermal, spectral, topographic and chemical data of the south seasonal and perennial caps, the SPLD, and the surrounding mantled terrains. They have helped to identify the different constituents (e.g., CO_2 and H_2O ices, particulated materials), their relative proportions, distribution, and seasonal behavior. *Kieffer* [1979] has shown that the south perennial cap is covered with CO_2 frost and *Kieffer* [1976] demonstrated that north polar cap is composed of water ice using temperature measurements made by the Infrared Thermal Mapper (IRTM). These data confirmed earlier discoveries based on telescopic observations and laboratory work [*Herr and Pimentel*, 1969; *Kieffer*, 1970; *Larson and Fink*, 1972]. The Mars Orbiter Camera (MOC), onboard Mars Global Surveyor (MGS), returned meters-scale images of the seasonal and perennial caps and helped to characterize the south polar environment. Among the most significant discoveries was the identification of erosive features (spiders, etched polygons) associated with what was subsequently hypothesized to be the basal sublimation of the translucent seasonal cap [*Piqueux et al.*, 2003; *Kieffer et al.*, 2006; *Kieffer*, 2007; *Piqueux and Christensen*, 2008b], and the identification of erosive depressions on the perennial cap [*Thomas et al.*, 2000; *Malin and Edgett*, 2001; *Malin et al.*, 2001; *Thomas et al.*, 2005]. These observations, together with THEMIS IR measurements of water ice temperatures at their floors [*Titus et al.*, 2003, 2004] were combined with thermal modeling [*Byrne and Ingersoll*, 2003], and showed that the southern perennial cap has a binary composition of CO_2 ice (8–10 m thin veneer) on a wider body of mostly buried frozen water.

[4] The Thermal Emission Spectrometer (TES) measured the temperature, albedo and the spectra of the polar ices [*Kieffer et al.*, 2000]. TES data suggested that the translucent cap region is due to CO_2 crystals that are large enough to be transparent at the visible wavelengths [*Kieffer et al.*, 2000]. The translucent ice is associated with the basal sublimation of the seasonal cap. Albedo and temperature measurements helped *Kieffer et al.* [2000] to determine the ice mass budget of the CO_2 caps. Topographic data returned by the Mars Orbiter Laser Altimeter (MOLA) [*Smith et al.*, 1999] have been used to constrain the mechanical properties of the SPLD, and show that they are likely composed of a mix of water ice and dust [*Nye et al.*, 2000]. In addition, MOLA has shown that the thickness of the seasonal CO_2 frost deposits to be 1–2 m [*Smith et al.*, 2001]. The integration of MOLA topography, Mars Express Mars Advance Radar Sounding and Ionosphere Analysis (MARSIS) mapping of the base of the SPLD, and high resolution gravity data made possible by the Mars Reconnaissance Orbiter flight configuration [*Zuber et al.*, 2007b] have been used by *Zuber et al.* [2007a] to calculate the density of the SPLD and determine that they are made of 85% water with ~15% dust by weight. MARSIS data confirmed that the SPLD are composed of almost pure water ice [*Plaut et al.*, 2007]. The Mars Odyssey Gamma Ray Spectrometer instrument suite has mapped the distribution of the subsurface water ice, only observed at the high latitudes [*Mitrofanov et al.*, 2002; *Boynton et al.*, 2002; *Feldman et al.*, 2004]. The first detection of exposed water ice near the south pole of Mars was made by *Titus et al.* [2003] using THEMIS data. *Bandfield* [2007] mapped the relative depth of the water ice table at the high latitudes using THEMIS measurements and thermal modeling. Observations of the seasonal cap by THEMIS and OMEGA also facilitated the understanding of the nature of the dusty and sandy spots and fans covering the seasonal cap on the translucent cap [*Kieffer et al.*, 2006; *Langevin et al.*, 2006; *Kieffer*, 2007]. Finally, THEMIS has mapped the changes of the distribution of the CO_2 ice composing the perennial cap [*Piqueux and Christensen*, 2008a; *Winfree and Titus*, 2007]. *Putzig and Mellon* [2007a] have mapped the thermal inertia of the south polar region and found an extensive region between 87°S and ~80°S with a very high thermal inertia (e.g., >1000 J m^{-1} K^{-1} $s^{-0.5}$, also called "I units" in this article) consistent with exposed or near surface water ice. OMEGA, onboard Mars Express, has provided the first spectral detection of water ice near the south pole [*Bibring et al.*, 2004] and constraints on the H_2O crystal sizes [*Douté et al.*, 2007]. The exposed water ice outcrops mostly near the CO_2 perennial cap. The map produced by *Bibring et al.* [2004] has a resolution of ~2 km and a partial coverage of the polar latitudes but most of the terrains pole-ward of 87°S are observed, which is not always the case for other instruments because of their polar orbit. CRISM has also identified the spectra of water ice near the region where THEMIS has first discovered water ice [*Titus et al.*, 2008].

[5] Most of the existing work has focused on the characterization of the ice volume in the SPLD. In this article, we extend the work of *Titus et al.* [2003] and map at 100 m per pixel, the highest resolution to date, the distribution of the ices near the south pole of Mars using THEMIS measurements.

3. Method

3.1. Data Selection

[6] The SPLD are free of seasonal frost during the summer, between Ls = 320° and 360° [*Kieffer*, 1976; *Kieffer et al.*, 2000; *Piqueux and Christensen*, 2008a]. We have selected THEMIS IR data taken during this time period (Table 1). Approximately 90% of the data selected for this study are taken between 325° < Ls < 345° and most are near Ls = 335°. The SPLD range from 90°S to 75°S. Because of the inclination of Mars Odyssey polar orbit, there are no data available between the south pole and 87°S. This study applies to the latitudes southward of 70°S but most of our figures and discussion do not further discuss the case of the terrains between 70°S and 80°S because we have determined that they are only covered with dust. We have only selected the "noon" side of the THEMIS images, i.e., the portion of the images with the highest sun elevation. In the early afternoon, the surface temperatures are higher than near midnight and the signal-to-noise ratio is higher. Typically, the local times of the THEMIS images selected for this work are composed of between 12.5 H and 16.0 H (24 H equals 1 Martian day), when the thermal contrast between the different surfaces is high (Table 1).

Table 1. THEMIS Data Used to Generate Figure 3

Image ID	Ls	Center Local Time (H)
I00826006	330	11.2
I01162002	345	13.2
I08963009	320	12.2
I09411008	341	9.9
I09424009	341	9.9
I09425008	341	9.9
I09438004	342	10.3
I17049007	308	8.3
I17151002	313	15.6
I17172005	314	15.0
I17283007	319	9.4
I17300009	320	6.7
I17413004	325	15.6
I17449009	327	14.8
I17485009	329	7.7
I17486013	329	7.6
I17487011	329	7.8
I17488016	329	6.7
I17489011	329	7.6
I17496009	329	7.9
I17534012	331	10.2
I17538010	331	10.3
I17539013	331	10.5
I17546015	331	14.4
I17560013	333	7.9
I17561012	332	15.0
I17562011	332	15.0
I17573010	333	8.9
I17575012	333	8.6
I17576011	333	8.9
I17584007	333	9.1
I17587005	333	10.6
I17588009	333	9.1
I17610012	334	14.9
I17613010	334	15.0
I17624010	335	15.0
I17625011	335	14.8
I17636011	335	15.0
I17658016	336	10.1
I17672013	337	7.7
I17675013	337	11.0
I17676013	337	7.2
I17687018	338	10.4
I17688018	338	7.9
I17708014	339	10.5
I17709014	339	10.4
I17711013	339	10.4
I17712014	339	10.4
I17713014	339	10.5
I17735014	340	10.5
I17750013	340	11.1
I17758017	341	6.2
I17785013	342	10.4

3.2. Thermal Modeling

[7] Polar materials (e.g., dust/sand, H_2O and CO_2 ices) are well characterized by their temperature and albedo [*Titus et al.*, 2003; *Piqueux and Christensen*, 2008a]. In this study, the identification of polar materials is based on the fit of temperature measurements made by THEMIS with the surface temperature prediction of a thermal model. The surface temperatures are found after solving for:

$$\varepsilon\sigma T_S^4 = S_M(1-A)\cos i + F_{IR} + L\frac{\partial m}{\partial t} + I\sqrt{\frac{\pi}{P}}\frac{\partial T}{\partial Z} \qquad (1)$$

with ε the emissivity of the surface, σ the Stefan–Boltzmann constant, T_s the surface temperature, S_M the insolation at the surface of Mars after atmospheric correction, A the albedo, i the solar incidence angle, F_{IR} the downwelling atmospheric radiation, L the latent heat of H_2O sublimation with m the mass ice to sublime, t the time, I the thermal inertia, P the diurnal period, T the subsurface temperature field, and Z the depth. The portion of the numerical code that models the atmospheric contribution are from H.H. Kieffer's KRC model [*Fergason et al.*, 2006]. The thermal inertia I is related to the thermophysical properties of the Martian materials by:

$$I = \sqrt{k\rho C_p} \qquad (2)$$

with ρ the density and C_p the specific heat. The model determines the surface temperature T_s from the thermal inertia. I is then interpreted in terms of composition or particle size when appropriate. The parameters for the thermal modeling are detailed in Table 2. They are either published values (e.g., water ice density, specific heat, thermal conductivity, etc.) or straightforward data provided by TES (surface albedo and emissivity, average atmospheric dust opacity, etc.).

[8] Our mapping technique does not allow us to detect water ice on the carbon dioxide perennial cap. Water crystals mixed within the perennial cap are at CO_2 ice temperature and cannot be detected based on their temperatures. In this specific case, the temperature of the water ice, and any other constituent of the perennial cap, is forced to remain at the buffered CO_2 temperature (148 K) and is not deterministic of the composition of the minor ice phase. In this article, we do not map water ice that is exposed at the surface of the CO_2 perennial cap; in all other cases, water ice is characterized by its temperature, even in the case of phase change. The diurnal temperature cycle of an ice, as well as its optical constants, are unique physical characteristics appropriate for unambiguous detection.

3.2.1. Apparent Temperature of Carbon Dioxide T_{CO_2}

[9] At a pressure of 7 millibars, the equilibrium temperature of CO_2 with respect to phase change is 148 K. At such temperatures, THEMIS accuracy is ~1 K [*Christensen et al.*, 2004]. The atmospheric correction algorithm we used [*Bandfield and Smith*, 2003] introduces a few K of error depending on the state of the atmosphere at the time of acquisition. In addition, the perennial cap is punctured by circular erosive depressions ("Swiss Cheese") whose floors are at water ice temperature (e.g., typically ~25 K warmer than CO_2 ice at Ls = 325°). As a result, subpixel mixing between carbon dioxide ice and warmer material occurs, and the apparent temperature of CO_2 ice of the cap is $140 < T_{CO_2} < 158$ K.

3.2.2. Apparent Temperature of Water Ice

[10] *Titus et al.* [2003] have shown that the sublimation of water ice near the south pole in the late summer does not absorb a significant fraction of the solar radiation (e.g., ~0.2%) and does not significantly lower the temperature of the ice (e.g., ~0.2 K). For this reason, the latent energy of sublimation of water ice is not considered and equation (1) becomes:

$$\varepsilon\sigma T_S^4 = S_M(1-A)\cos i + F_{IR} + I\sqrt{\frac{\pi}{P}}\frac{\partial T}{\partial Z} \qquad (3)$$

Table 2. Parameters Used for the Thermal Modeling (Figure 1)

Parameter	Value	Note
Albedo H_2O	0.25	TES data, *Titus et al.* [2003] chose 0.30
Albedo sand	0.23	TES data, *Titus et al.* [2003] chose 0.30
Albedo dust	0.23	TES data, *Titus et al.* [2003] chose 0.30
k H_2O	3.42 W/m/K	*Hobbs* [1974]; *Titus et al.* [2003]
k Dust	0.004 W/m/K	*Presley and Christensen* [1997]
k Sand	0.099 W/m/K	*Presley and Christensen* [1997]
C_p H_2O	7,001 × T + 167,55 J/K/kg	*Hobbs* [1974]; *Giauque and Stout* [1936]
C_p dust	420 J/K/kg	Assume a porosity of 0.50
C_p sand	538 J/K/kg	Assume a porosity of 0.36
Dens H_2O	944,73 − 0,0991 × T kg/m^3	*Hobbs* [1974]
Dens dust	1500 kg/m^3	Assume a porosity of 0.50
Dens sand	1920 kg/m^3	Assume a porosity of 0.36
Thermal inertia H_2O	2128 I unit	Assumes T = 180 K
Thermal inertia dust	320 I unit	
Thermal inertia sand	50 I unit	
Surface emissivity	0.99	
Latitude	83°S	Median latitude
Solar longitude Ls	335°	Median Ls
Dip	0°	Flat surface
Strike	0°	Flat surface
Average atmospheric radiative temperature	165 K	Estimated with a grey 1 layer atmosphere
Dust vertical opacity	0.2	*Titus et al.* [2003]

[11] Water ice has the highest thermal conductivity and inertia among geological materials observed at the surface of Mars [*Titus et al.*, 2003, Table 2]. As a result, its diurnal temperature variation is characteristically small. Massive bedrock may have a somewhat similar value of thermal inertia, e.g., above 1200 I units [*Kieffer et al.*, 1973] versus >2000 I units for H_2O, occasionally resulting in similar temperatures, but the SPLD and the surrounding mantled terrains, composed of hundreds of meters to kilometers of dust and ice deposits [*Murray et al.*, 1972; *Soderblom et al.*, 1973; *Cutts*, 1973; *Blasius et al.*, 1982; *Milkovich and Head*, 2005], are not expected to display bedrock exposures. We have determined, using TES data, that polar terrains with such high thermal inertias have a typical albedo of 0.25. This is the albedo we assign to water ice in the rest of this article and for the thermal modeling. At Ls = 335°, and using the parameters given in Table 2, we find that exposed water ice temperature is always close to 177 K and always significantly higher than the temperature of CO_2 ice (Figure 1A). Earlier and later in the season, at Ls = 325° and Ls = 345°, water ice still remains >20 K warmer than CO_2 ice (Figures 1B and 1C). To account for the latitudinal variations within the study area, we have calculated the temperature of exposed water ice at different latitudes and show two examples at 87°S and 80°S (Figures 1D and 1E). The shift of temperature due to the variation of latitude is ±2 K, with temperatures ranging from 176 K to 180 K at noon. We have also investigated the effect of different surface albedos because some variations may be expected as a function of the dust content of the ice. For surface albedo changes of up to 15% (e.g., 0.23 to 0.27), Figures 1F and 1G show that the effect on the surface temperature is very small (<1 K). Finally, we have computed the effect of sloping surfaces on the thermal diurnal cycle. Near the south pole and during the summer, the peak temperature of sloping surfaces occurs at a different local time as a function of the azimuth and slope. The thermal diurnal amplitude does not fundamentally change. Beyond 10° of slope, the thermal diurnal cycle gets significantly delayed or advanced and afternoon water ice temperatures are ∼175 K, which is close to the temperature of dust (Figure 1H). Therefore the surface material identification may not be accurate where slopes exceed 10°. Beyond 10° of slope, our mapping technique is not appropriate and a model taking the topography into account is required. These terrains correspond to the edges of the SPLD and the walls of the polar troughs, and together, they represent ∼1% of the total surface area between 70°S and the pole.

3.2.3. Apparent Temperature of Particulate Material

[12] Fine dust (I ∼ 50) is also expected at the surface of the SPLD [*Titus et al.*, 2003]. SPLD dust albedo is 0.23 [*Titus et al.*, 2003]. Dust does not conduct heat as efficiently as ice or sand [*Presley and Christensen*, 1997] and large surface diurnal thermal amplitudes are expected, with hotter temperatures than water ice near noon (189 K, Figure 1A) and cooler near midnight (168 K). We have calculated the temperature of dusty surfaces in a variety of conditions, between Ls = 325° and Ls = 345°, for latitudes ranging from 87°S and 80°S, with surface albedo of 0.21 to 0.25 and with sloping surfaces (Figure 1). Under this range of conditions, dusty surfaces in the afternoon are always significantly hotter than CO_2 ice (by at least 15 K) and temperatures alone are sufficient to distinguish dust and CO_2 ice.

[13] Near 7 am and 6 pm (for flat surfaces), the temperature of the dusty surfaces are similar to those of exposed water ice surfaces, typically near 177 K (Figure 1A). At these local times, thermal data are not appropriate to distinguish between dust and water ice. We have eliminated the portions of the THEMIS images near these local times in this study and only use the noon side of the images. Under these conditions, dust is typically hotter than 180 K which is significantly warmer than both water and CO_2 ices.

[14] Sand size particles (I ∼ 250) may also be present at the surface of the SPLD [*Kieffer et al.*, 2006; *Kieffer*, 2007; *Piqueux and Christensen*, 2008b]. The material probably brought to the surface of the seasonal cap by jets is consistent with sand size particles [*Kieffer*, 2007; *Piqueux and Christensen*, 2008b] and indicates that patches of sandy material may be covering parts of the SPLD. Thermal

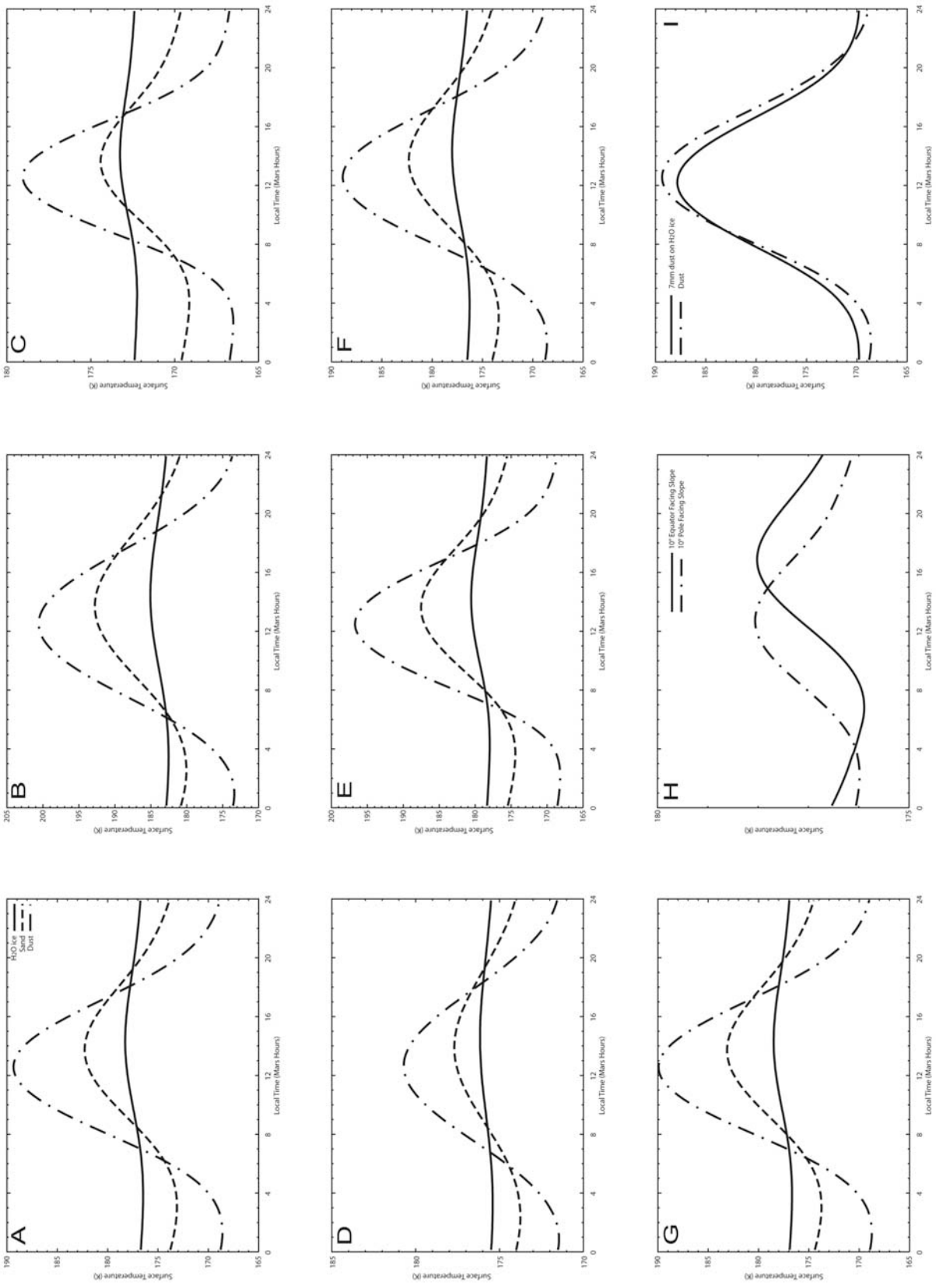
A
B
C
D
E
F
G
H
I
H2O Ice
Sand
Dust
7mm dust on H2O ice
Dust
10° Equator Facing Slope
10° Pole Facing Slope
Surface Temperature (K)
Local Time (Mars Hours)

Figure 1

modeling indicates that sandy surfaces will always be hotter than CO_2 and H_2O ice temperatures between 8 am and 7 pm (Figure 1).

[15] Because this work focuses on the water ice distribution, and because modeling indicates that the temperatures of sand and dust on one hand, and the temperature of H_2O ice on the other hand, are always significantly different, we do not differentiate dusty and sandy surfaces in the remaining of the text and in the figures. We chose to name "dust" any bare surface, free of CO_2 and H_2O ices.

3.2.4. Layered Material

[16] *Titus et al.* [2003] have shown that the temperature of the particulated surface of an area of the SPLD is best modeled with a layer of dust lying on a water ice substrate. Data from the Mars Odyssey neutron spectrometers are consistent with large fractions of water ice in the near subsurface [*Mitrofanov et al.*, 2002; *Boynton et al.*, 2002; *Feldman et al.*, 2004] and a thermal study by *Bandfield and Feldman* [2008] indicates that water ice is only covered with a shallow layer of particulate material. For completeness, we have calculated the diurnal temperature cycle of layered surfaces (e.g., dust on water ice) for a variety of conditions. Dust on water ice results in thermal diurnal cycles that are significantly different from exposed water ice but similar to pure dust [*Putzig and Mellon*, 2007b]. Figure 1I shows the diurnal cycle of pure dust versus 7 mm of dust on water ice. *Titus et al.* [2003] found that this is the configuration that best models the thermal seasonal cycle on the area they studied. Again, at 7–8 am and 5–7 pm, layered, dusty/sandy and water ice surfaces display similar temperatures, and data acquired near these local times have been avoided.

3.2.5. Subpixel Mixing

[17] In some cases, measured temperatures cannot be matched with modeled temperatures. We assume that subpixel mixing between CO_2, water ice, or particulate material is responsible for this behavior. These pixels are typically located at the margin of the CO_2 cap or at the periphery of troughs and depressions in the perennial cap, and are therefore consistent with subpixel mixing of CO_2 ice and other hotter materials. In most cases, these pixels are also located near exposed water ice, suggesting that intermediate temperatures correspond to the subpixel mixing of CO_2 and H_2O ice with no dust involved.

[18] In theory, the right mixture of dust and CO_2 ice can result in temperatures similar to that of H_2O ice. However, mid-summer adjacent CO_2 ice and dusty surfaces are not stable because of their large temperature differences: 2–3 days after a particulated surface has been freed from its cover of seasonal frost, its temperature has increased by 30–80 K (mostly depending on the slope orientation), making any stable close contact with CO_2 ice impossible.

Figure 1. Plot of the modeled diurnal temperature curve for H_2O ice, sand and dust using the parameters given in Table 2 and the legend of Figure 1A (unless specified). (A) The difference in surface temperature between the exposed materials is larger near noon and midnight, i.e., 15 K between dust and water ice, making their identification unambiguous. For this study, only data acquired near noon are considered because the temperatures and therefore the signal-to-noise ratio are higher. (B) Diurnal variations at Ls = 325°, a few Martian days after the removal of the last seasonal CO_2 frost. The large majority of the data used in this study have been acquired after Ls = 325°. Near this time of the season, the thermal contrast between the surface materials is the highest and their identification the easiest. Data acquired between 8.0 H and 17.0 H are appropriate. As the season advances, the sun elevation is lower and the thermal contrast decreases. (C) Diurnal variations at Ls = 345°, the latest time in the season for the data selected to map the distribution of the surface material. At Ls = 345°, the surface materials are much cooler than earlier in the season, but still at least 15 K hotter than CO_2 ice. Near noon, the thermal contrast between H_2O ice and dust is only 6 K, which is sufficient to identify the surface material, but data must be acquired sufficiently close to the local noon (±2 hours). Figures 1B and 1C show that between Ls = 325° and Ls = 345°, H_2O ice can be identified with its temperature. (D) Diurnal variations at 87°S of latitude, the highest latitude accessible with THEMIS data. Closer to the geographic pole, less solar illumination hits the surface, resulting in lower thermal contrast between different surface materials. This plot indicates that near noon, dusty surfaces are significantly warmer than water ice surfaces (e.g., 5 K) and that thermal mapping is possible even at the highest latitudes. However, the data selection must be more constrained than at other latitudes for optimum results (e.g., data acquired as early as possible in the season and near 12 H). Because THEMIS images the latitudes near 87°S 12 times a day, large quantities of data are available and severe constraints on the local time and season are not crippling. (E) Diurnal variations at 80°S. At these latitudes, the sun is only a few degrees above the horizon during the summer. This is sufficient to generate a substantial temperature contrast between H_2O and dust (e.g., 20 K). Figures 1D and 1E demonstrate that at any latitude, H_2O ice can be identified with its temperature. (F) Diurnal variations with higher albedos than those given in Table 2 (+0.02). When compared with Figure 1A, Figure 1F shows that an increase of the surface albedo does not significantly change the temperature. (G) Diurnal variations with lower albedos than those given in Table 2 (−0.02). Figure 1G can be compared with Figures 1A and demonstrates that large variations of surface albedos (i.e., 15% modeled here) are not significantly changing the surface temperatures. (H) Diurnal variations for a 10° slope facing the equator and the pole. Slopes tend to modify the diurnal thermal amplitude and the time of the maximum and minimum temperature. Near the south pole, the main effect is an apparent change in the local time of the extreme temperatures. Figure 1G indicates that the apparent local time can be switched to several hours because of slopes. (I) Diurnal variations for pure dust and a 7-mm layer of dust on water ice. The SPLD are likely made of a large body of frozen water covered with a thin layer of dust. *Titus et al.* [2003] found that the best fit between the temperature measurements and a model was obtained with a 7-mm layer of dust on a large body of water ice. This plot shows that the temperature of dust on water behaves similarly to the temperature of pure dust. Even a few hundreds of micrometers of dust on water would significantly change the apparent temperature of such a surface compared to that of pure water ice.

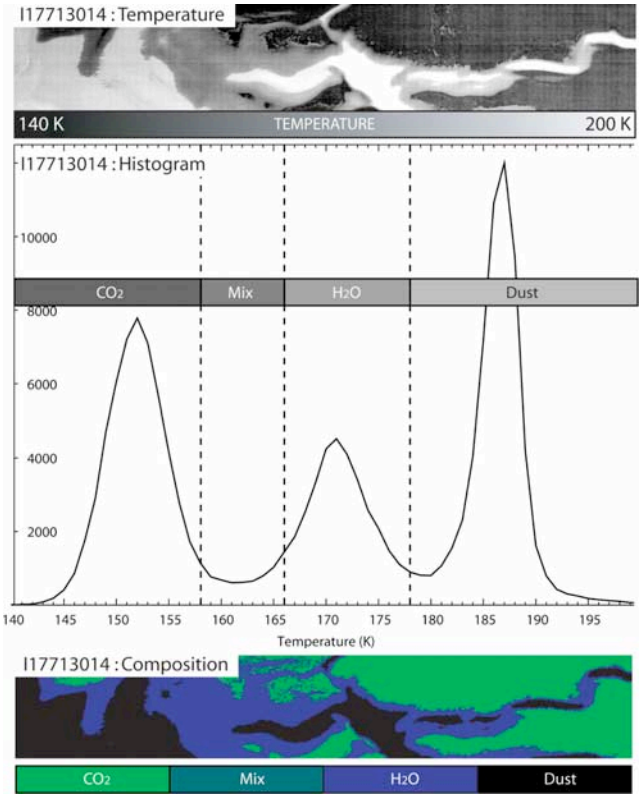

Figure 2. Schematic of the thermal mapping procedure: the THEMIS images are converted into temperatures corrected from atmospheric effects. The image histogram displays several thermal domains. These domains are CO_2 ice, water ice, dust/sand and mixed materials. After assigning each temperature measurement (i.e., pixel) with a thermal domain, a composition image is generated. The THEMIS image used for this example is I17713014.

We have only selected data acquired in the mid-summer, many days after the CROCUS date, in order to only observe seasonally stable surfaces, e.g., surfaces where the CO_2 ice is stable and not retreating. As a consequence, CO_2 ice and dust subpixel mixing, leading to a possible erroneous identification of water ice is unlikely. Thanks to its high thermal inertia resulting in small thermal gradients, H_2O ice is form transition areas between the perennial CO_2 cap and the dust, resulting in areas where dust, H_2O and CO_2 ice are present in a single THEMIS pixel. These pixels have been mapped as ''mixed'' materials. In addition, the south polar region is imaged 12 times a day, every day, allowing us to observe each location at different local times. This wealth of data was used for any given location to verify the consistency of our original mapping with data acquired at other local times, reducing the possibility of mapping errors. Erroneous identifications of exposed water ice cannot be repeated several times a day because subpixel mixing results in diurnal (and seasonal) thermal variations that are very different from thermal variations of pure H_2O ice. Subpixel mixing of various materials can result in the same apparent temperature as exposed water ice only at specific local times, but not all day long. We take advantage of the uniqueness of the diurnal curves to prevent misidentifications of exposed water ice.

3.2.6. Mapping Example

[19] For each temperature measurement (i.e., THEMIS pixel), we have assigned a surface composition (i.e., CO_2 ice, H_2O ice and dust) based on the thermal modeling presented above. Four types of surfaces have been identified, i.e., CO_2 ice, H_2O ice, dust, and mixed surface materials whose temperatures cannot be assigned to a single material. An example of mapping for a single THEMIS image is provided on Figure 2. Thermal modeling of the surface materials indicates that 145 K < T_{CO_2} < 158 K, 166 K < T_{H_2O} < 178 K, and 178 K < T_{dust}. The histogram of this image displays these three domains, centered at 152 K, 172 K and 187 K (Figure 2). The domain between 158 K and 166 K corresponds to a mix of different surface materials, resulting in intermediate temperatures. Typically, these intermediate temperatures are measured on extremely small fractions of the images, e.g., 5% on Figure 2. Only 0.3% of the terrains between 87°S and 80°S display mixed materials temperatures (and none southward of 80°S). The lower part of Figure 2 represents the composition map generated from the thermal and histogram analysis. By extending this process to the latitudes between 87°S and 70°S, we have divided every image's histogram in four thermal domains, assigned a composition to each (i.e., CO_2 ice, mixed material, H_2O ice and dust), and constructed the map of the distribution of the surface material (Figure 3).

4. Results and Discussion

4.1. Water Ice Distribution

[20] A map of the surface material near the south pole based on THEMIS surface temperature measurements is presented on Figure 3. 40,000 km^2 of exposed water ice are identified near the south pole. The exposed water ice is observed: (1) on the SPLD, at the margin of the perennial cap, forming a region of transition between the dusty surfaces and the CO_2 ice of the perennial cap; and (2) forming a 300 km by 80 km patch centered at 345°E and 83.5°S on the southern high latitude mantled terrains. This patch represents the largest continuous exposure of water ice on Mars other than the north polar cap. Near 335°E, 83.5°S the exposure of H_2O is fragmented in ~10 patches covering ~700 km^2 each. The equator-most outcrop of water ice is visible in the floor of a shallow unnamed crater centered at 80.2°S and 5°E.

4.2. Correlation of Water Ice Occurrence and Surface Albedo

[21] *Titus et al.* [2003] first noticed a correlation between the nature of the surface material and the albedo. *Bibring et al.* [2004] also observed this correlation for a larger surface area. The distribution of water and CO_2 ices (Figure 3) closely matches *Herkenhoff*'s [2001] Unit Af of the Martian south polar region geologic map based on albedo and color images from Viking. Herkenhoff interpreted this Unit (Af) to be patches of partially defrosted terrains. We have compared the distribution of the ices and dust with regional albedo data and we confirm the correlation reported by *Titus et al.* [2003]. Figure 4 is an example of correlation between surface composition and albedo. The fact that water ice has

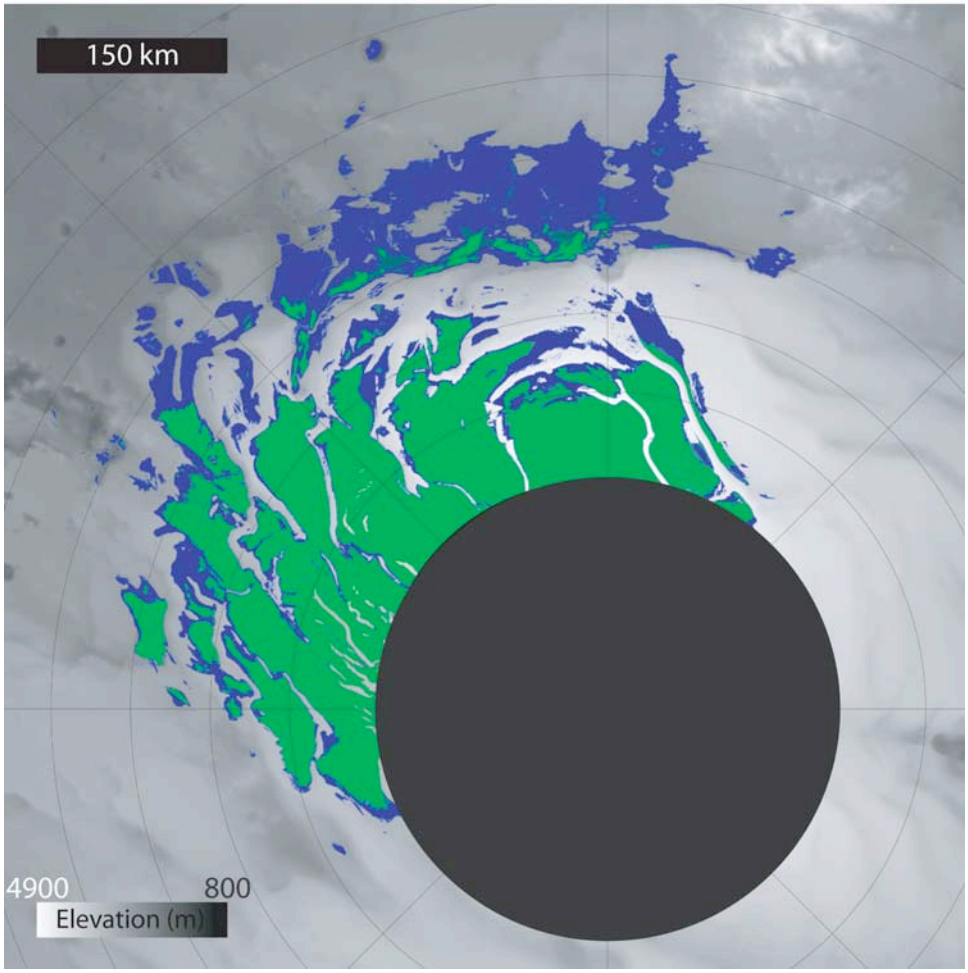

Figure 3. Distribution of the exposed surface material near the south pole between Ls = 325° and Ls = 345°. The black circle indicates the region where no data are available. Latitude and longitude grid is every 1° and 45°, respectively. Perennial CO_2 ice is mapped in green and H_2O ice in blue. Other surfaces are covered with dust. The background is a grey scale MOLA elevation model. Most of the exposed water ice is not observed on the SPLD, but on the surrounding mantled terrains. Notice that OMEGA and CRISM have detected small quantities of H_2O ice on the CO_2 perennial cap not shown here. Data are from Table 1.

a remarkably constant albedo indicates that it has a homogeneous crystal size and dust fraction. *Douté et al.* [2007] found a typical H_2O crystal size of 150 μm using OMEGA and *Titus et al.* [2003] calculated that the typical south polar albedo of water ice may be due to a combination of 8 to 80 μm ice crystals and a dust fraction of 0.01% to 10%. In addition, the albedo boundaries observed on the THEMIS VIS and MOC images are similar to those recorded by Viking (resolution variable, typically near 90 to 900 m per pixel) and Mariner 9 (resolution of a few tens of meters per pixel, incomplete coverage) indicating that the distribution of water ice has not significantly changed since 1972.

4.3. Comparison With OMEGA

[22] In those regions of the south pole where OMEGA data were available, *Bibring et al.* [2004] used spectroscopic methods to identify H_2O ice. Where the coverage overlaps, our map is consistent with the H_2O ice detection by OMEGA [*Bibring et al.*, 2004]. A detailed comparison is limited by the difference of coverage (incomplete mapping by OMEGA between 87°S and 70°S and absence of coverage by THEMIS between 90°S and 87°S). Where both instruments have mapped the distribution of the ices, we note the following:

[23] 1. The water ice exposures detected by OMEGA on the SPLD and the surrounding mantled terrains are also present on Figure 3 suggesting a good agreement between the 2 different mapping techniques.

[24] 2. More small patches of water ice are mapped with thermal data on Figure 3 (in particular near 343°E 84.9°S). The non-detection of some outcrops of water ice can be due to the lower spatial resolution of OMEGA at the time of the mapping phase compared with THEMIS IR (1 OMEGA pixel corresponds to ~400 THEMIS pixels) inducing some dilution of the signal. Alternatively, it is possible that these regions were covered with a very thin dust veneer. Figure 5 shows two of these regions, having the characteristic temperature of water ice but no spectral feature on OMEGA

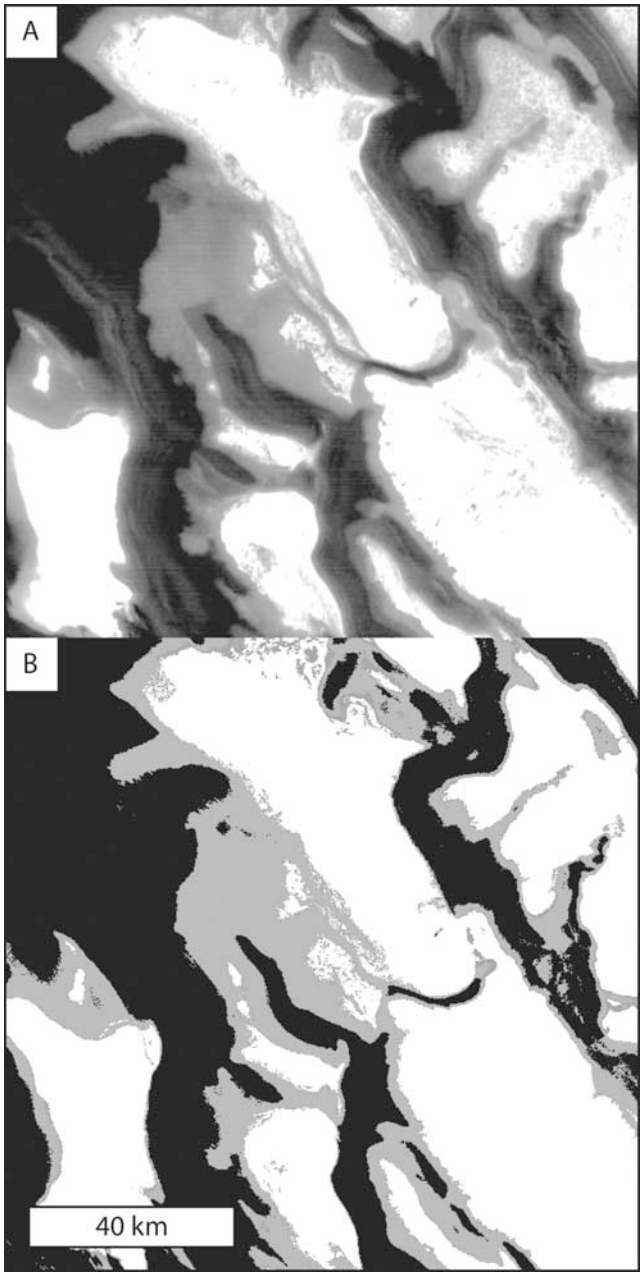

Figure 4. Correlation between (A) albedo and (B) surface composition. The albedo is from M1400555 (Ls = 333°, 283.93°E, 84.90°S). Figure 4A has been stretched to enhance the albedo boundaries. On the composition map, CO_2 ice is mapped in white, H_2O ice in grey, and dust in black. At the regional scale, we find an excellent correlation between the albedo and the surface composition mapped on Figure 3.

data. These patches have an albedo higher than the surrounding dust (Figure 3) consistent with that of water ice.

[25] 3. None of the water ice on the CO_2 perennial cap imaged by OMEGA is present on Figure 3. Water ice on the perennial cap is at CO_2 ice temperature (e.g., ~148 K) and is forced to stay at this temperature, without diurnal variations. In this case, the temperature of the water ice is not a function of its physical characteristics as defined in equations (2) and (3) (i.e., albedo, density, specific heat and thermal conductivity) but is maintained at the buffered temperature of CO_2 ice.

4.4. Ground Patterns

[26] *Mellon* [1997] has shown that polygonal landforms should form at the high latitudes of Mars because of the seasonal thermal expansion and contraction of the water ice rich regolith. *Mangold* [2005] has mapped the distribution of these polygonal features and *Mangold et al.* [2004a] have shown that polygons occur mainly on water ice rich terrains as detected by the Neutron Spectrometer onboard Mars Odyssey. *Bibring et al.* [2004] observed the presence of polygonal features on exposed water ice. *Mangold et al.* [2004a], *Mangold* [2005] and *van Gasselt et al.* [2005] have previously mapped or classified the polygonal patterns based on their morphologies.

[27] We have mapped the distribution of the small-scale polygons (e.g., 50–200 m in size, Figure 6) near the south pole using MOC images and compared it with the occurrence of exposed water ice (Figure 7). We have observed a correlation between the occurrence of a specific type of polygons and exposed water ice. These polygons are outlined by ~50 m to subpixel resolution (i.e., a few meters) wide sides, and do not show any apparent topography (Figure 6). These polygons are located near the margin of the exposed water ice, near the transition with dust covered surfaces, and are outlined by a material having the albedo of dust. The dark outlines of the polygons may correspond to troughs caused by the preferential sublimation of H_2O ice along thermally

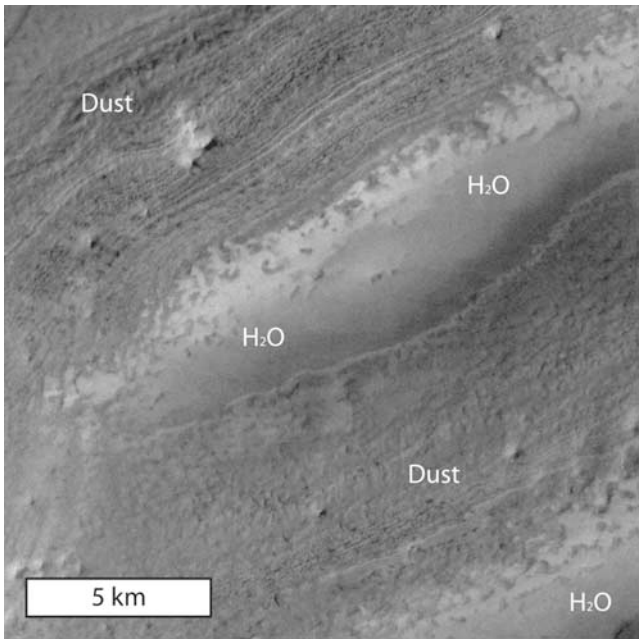

Figure 5. Detail of a region where temperatures are consistent with exposed water ice and dust. These patches are characterized by a higher albedo and a smoother surface than the surrounding dust. The water ice is punctured with bumps of underlying darker material, suggesting that H_2O ice does not form a thick (e.g., tens of meters) unit. V17736017, 84.54°S, 344.60°E, Ls = 339.9°.

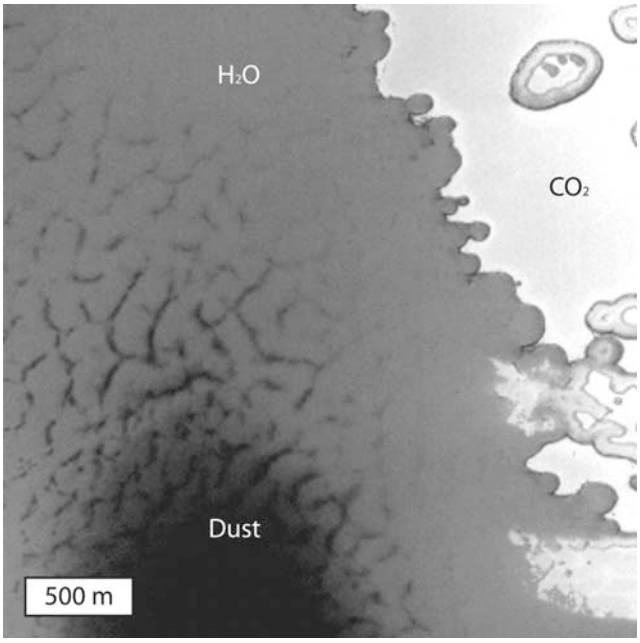

Figure 6. Polygonal ground patterns on exposed water, near the CO_2 perennial cap and dust. This class of polygonal patterns with dark, wide, and diffuse outlines is the only type that seems to be correlated with exposed water ice. They only represent a small fraction of the features mapped on Figure 7. Image R1304241, 280.67°E, 85.38°S, Ls = 341°.

stressed induced fractures [*Marchant et al.*, 2002] and filled up with loose and mobile material (dust, sand, pebbles).

[28] Other types of polygonal features do not correlate with the exposure of water ice (Figure 7). *Mellon*'s [1997] model of formation of the high latitude polygons requires the regolith to contain some fraction of water ice, but does not require the water ice to be exposed. Therefore the lack of systematic correlation between the distribution of the polygonal ground patterns and the exposed water ice is not inconsistent with the theoretical model of formation. In addition, *Piqueux and Christensen* [2008b] have shown that a class of patterned ground (''etched polygons'') are formed (or at least widened) by the scouring power of the migrating CO_2 gas that originates from the basal sublimation of the seasonal cap on the region where the carbon dioxide ice is translucent [*Kieffer et al.*, 2006; *Kieffer*, 2007]. Since these ground patterns are associated with the seasonal CO_2 ice, they are not expected to correlate with water ice, exposed or buried.

4.5. Timing Variability of the Condensation and Sublimation of the Seasonal CO_2 Ice

[29] The CROCUS date is defined by *Kieffer et al.* [2000] for a given location as the date when the last seasonal CO_2 frost sublimes, unveiling the underlying surface material. The terrains near the polar cap are typically free of CO_2 ice by Ls = 300° [*Kieffer et al.*, 2000]. However, for the next ~10°Ls, a layer of seasonal CO_2 frost does remain on surfaces where water ice is exposed later in the summer (Figure 8). There is a clear correlation between the distribution of water ice and the CROCUS date, i.e., the date at which the last seasonal frost is removed. The time of the earliest frost deposit, and therefore the thickness of the CO_2 deposit, may be a function of the substrate properties [*Haberle et al.*, 2008]. The earlier the surface gets frosted, the more CO_2 ice will accumulate during the fall. THEMIS thermal observations acquired a few Martian days before the beginning of the polar night (~Ls = 0°), indicate that the exposed water ice is at or near CO_2 condensation temperature whereas dusty surfaces are not (Figure 9). As a result, exposed water ice reaches the CO_2 condensation temperature before dusty surfaces do, and water ice surfaces start to accumulate frost a few days earlier. Data acquired near Ls = 10° indicate that all surfaces are covered with CO_2 frost at this date. After the sunset or at extremely low solar illumination angles, the advantage of THEMIS temperature measurements is crucial over other techniques (reflected solar light remote sensing) in order to identify and map the composition of the polar surface materials. We have determined that near the beginning of the polar night, exposed water ice is first covered with CO_2 frost and should accumulate more frost than dusty surfaces. This is consistent with the observation of the delay of the CROCUS date over terrains where water ice is exposed during the summer.

[30] *James et al.* [1987] compared telescopic data of the retreat of the south seasonal cap acquired throughout the 20th century. They found some variability, possibly associated with dust storms, but the overall result of this study was that the retreat of the seasonal cap has followed the same longitudinal and latitudinal assymetrical pattern since 1903 (year of the oldest set of observations used by James et al.). *Piqueux and Christensen* [2008a] have also shown that the retreat of the cap has been almost identical in 1894 (observations by *Lowell* [1896]) when compared to TES observations of the 1999 retreat. Because the timing and the shape of the retreating seasonal cap are strongly controlled by the occurrence of exposed water ice (among other parameters such as latitude, local slope, wind field, occurrence of dust storms, [*Kieffer et al.*, 2000]), it is likely that the similarity of the observations since 1894 indicate that water ice has been exposed in the same locations since at least the end of the 19th century.

4.6. Water Ice Thickness

[31] Our thermal models assume that the water ice layer is at least several diurnal skin depths thick. The diurnal skin depth δ is defined by:

$$\delta = \sqrt{\frac{kP}{\rho C \pi}} \tag{4}$$

giving $\delta > 25$ cm for H_2O ice on Mars. If the water ice layer was several times thinner than δ, the surface temperature measured would be detectably warmer than the outputs of our thermal models. The agreement between the measurements and the models indicate that the layer of exposed water ice mapped on Figure 3 is approximately a skin depth thick or more.

[32] THEMIS VIS (18 m per pixel) and MOC (a few meters per pixel) images of the exposed water ice terrains indicate very uniform surface characteristics. The water ice patches show little surface roughness at these scales, in

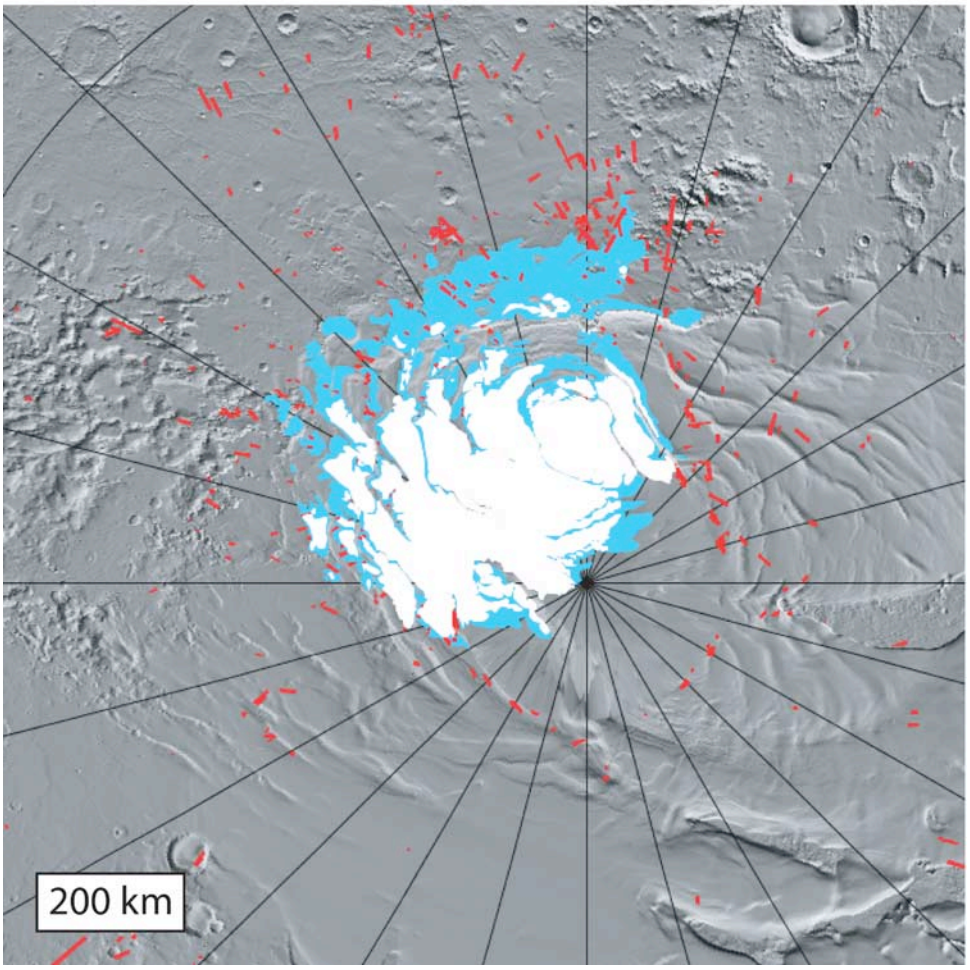

Figure 7. Distribution of small-scale polygonal features (red) near the south pole using MOC narrow angle images. The perennial CO_2 is mapped in white and the water ice in blue. Composition mapping between the pole and 87°S is based on MOC wide-angle albedo. The background is a MOLA-shaded relief map. Longitude lines are every 15°.

contrast with the adjacent dusty surface (Figures 4, 5, 6, 10; also see *Mangold et al.* [2004b]). However, at higher spatial resolution, HiRISE images indicate that water ice surfaces are locally shaped by very small-scale (meter) polygonal landforms. Figure 11 is a HiRISE view of the water ice floor of a ''Swiss Cheese'' feature. It shows a dense network of polygons outlined by CO_2 seasonal frost remaining in the troughs. It is not known at this time if these features are common because such small formations are only accessible on HiRISE images. On Figure 5, the low albedo smooth unit (e.g., H_2O) is punctured by a series of modest dark buttes, rising above the surrounding surface, suggesting that the water ice deposit is thin compared to the local surface topography (a few meters at most). This is consistent with the prediction of *Montmessin et al.* [2007] that the southern exposed water ice is a meters-thick layer at most. We have generated a series of MOLA topographic profiles in numerous places at the contact between the exposed water ice and the surrounding dust and we have not detected a difference of elevation between the two units (Figure 12) indicating that the thickness of the water ice unit is at or below the detection limit of MOLA (e.g., a few meters).

[33] Depending on the location, the boundary between water ice and dust can be either gradual or sharp (Figure 10). Where the compositional boundary is gradual, sub-circular patches of dark albedo material surrounded by water ice are observed. This dark material has an albedo that is consistent with dust, possibly indicating that the water ice layer is thin and punctured in places, forming windows where the underlying dust-rich terrain is visible. Alternatively, these dusty patches could be depressions where particulate material can accumulate on the water ice. Available data are not sufficient to distinguish these hypotheses, and it will be important to determine the thickness of the water ice layer exposed at the surface because it can provide fundamental constraints on the recent past and present polar environment.

4.7. Water Ice Stability and Long Term Evolution

4.7.1. Sublimation Rates

[34] It is difficult to calculate the amount of water that sublimes every summer because the state of the atmosphere near the surface is not known. *Smith* [2002, 2004] observed that the polar spike of the TES derived water vapor concentration (30–40 μm) starts well before Ls = 300°,

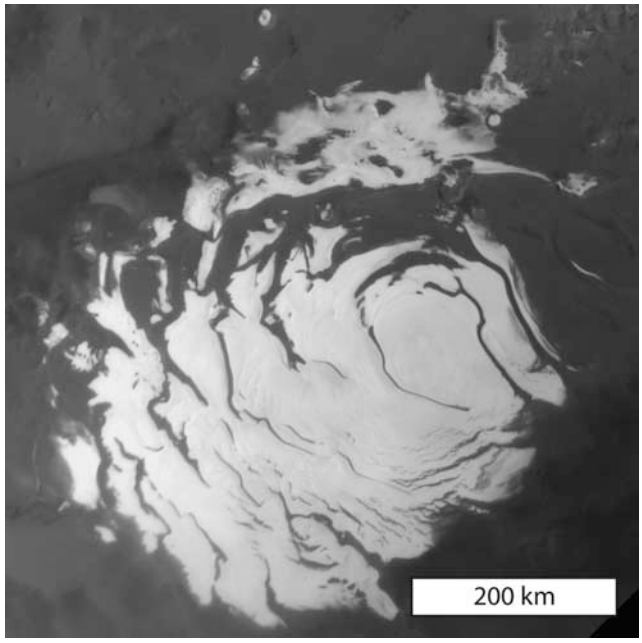

Figure 8. Last seasonal frost near the polar cap at Ls = 307°. Image R1104268. There is a clear correlation between the persistence of the last seasonal frost and the distribution of the exposed water ice (Figure 3).

when the water ice is not yet exposed (Figure 8), indicating that the contribution of the exposed water ice to the atmospheric vapor content is minor. After Ls = 310°, when the H_2O ice is exposed and sublimates, the vapor concentration above the cap has already significantly dropped (20–30 μm), further indicating that the exposed water ice is not a significant contributor to the atmospheric vapor, and that other sources are more important, e.g., the release of water trapped in the retreating southern CO_2 seasonal cap [*Pimentel et al.*, 1974] and the diffusion of vapor throughout the regolith [*Jakosky and Farmer*, 1982; *Jakosky*, 1983a]. In the late summer, near Ls = 325°, the exposed water ice surface temperature is maximal (T > 180 K) and the sublimation rate is also likely reaching its maximum value. At this time, the concentration of vapor in the atmosphere has dropped to ~10 μm (or less) near the pole, which is a common southern hemisphere vapor concentration above surfaces where water ice sublimation may not contribute, further indicating that the exposed water ice is a minor source of atmospheric vapor.

[35] Assuming that most of the sublimation occurs during the 10 Martian days when the exposed water ice is the hottest, i.e., near Ls = 325° when T > 180 K (Figure 1), that this water vapor is evenly diluted between 80°S and 90°S and represents 10 precipitable μm as measured by TES [*Smith*, 2002, 2004], and that the water column is refilled every day [*Jakosky and Farmer*, 1982; *Smith et al.*, 2002; *Titus et al.*, 2003], 1×10^8 m^3 or 1×10^{11} kg of water are lost every summer and injected in the atmosphere. For comparison, this is two orders of magnitude less water than the total amount in the atmosphere. Now let us assume that the atmospheric vapor only originates from the sublimation of surface water ice. The vertical erosion rate would be ~200 μm per day or ~2 mm per season. This is significantly higher than rates previously calculated for both polar caps (i.e., 100–800 μm per season by [*Ingersoll*, 1970; *Toon et al.*, 1980; *Haberle and Jakosky*, 1990; 10 μm per day for *Titus et al.*, 2003]) and not realistic since we have shown that the exposed water ice is not the main source of the southern atmospheric vapor.

4.7.2. Origin of the Water

[36] *Montmessin et al.* [2007] discuss in detail the possible origin of the water ice deposits observed by *Titus et al.* [2003] and *Bibring et al.* [2004] near the south pole of Mars. These authors favor a scenario where a meters-thick layer of H_2O was deposited ~21,500 years ago when the perihelion was synchronized with the northern summer. Under these conditions, the north H_2O cap was unstable

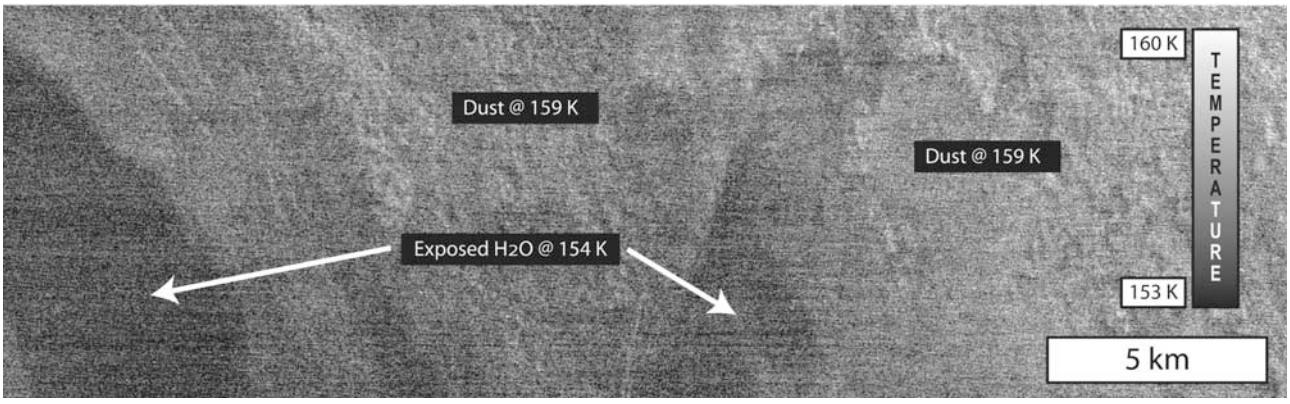

Figure 9. Surface temperature on the SPLD at the beginning of the fall (Ls = 0°), when the sun is only rising 4° above the horizon at noon. On this image taken at 14 H, the warmest time of the day, the dusty surfaces (brightest pixels, ~159 K) are 5 K warmer than the patches of exposed water ice (~154 K), which are at or slightly above the carbon dioxide condensation temperature. THEMIS measurements indicate that exposed water ice surfaces reach the CO_2 frost condensation temperature earlier in the fall and can start accumulating frost several Martian days before dusty surface do. Because more CO_2 ice condenses on exposed water ice surfaces, it takes more energy to sublime it in the spring, delaying the CROCUS date. Image I0152202, 80.5°S, 24.70°E.

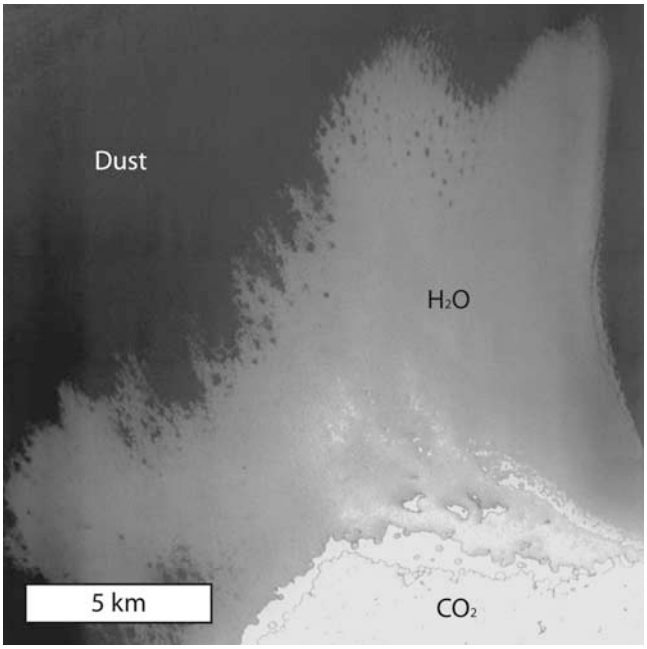

Figure 10. Relationship between the CO_2 and H_2O perennial caps and the dusty surface of the SPLD. The transition between the dust and the H_2O ice is either sharp or irregular and transitional, with isolated patched of dust albedo material on the ice. V17551011, 84.4°S, 282.1°E, Ls = 332°.

and released massive amounts of vapor in the atmosphere. Global atmospheric circulation modeling indicates that the vapor was transported to and deposited near the south pole at a rates as high as 1 precipitable mm per year, able to quickly form a thick cover of water ice. Since then, the perihelion has switched to the current values and the mantle of exposed water ice is no longer stable and sublimes. The original meters-thick deposits have thinned and retreated to the extent observed today.

4.7.3. Fate of the Water

[37] Once transferred to the atmosphere, water vapor may have several destinations. First, it can be cold-trapped on the south perennial cap. At 148 K, the partial pressure of water vapor in equilibrium with the frost is 10^{-7} mbar, several orders of magnitude less than the vapor content of the atmosphere, indicating that H_2O will condense on the CO_2 cap and stay until the cap is removed, during periods of high obliquity for example. The spectral signature of water ice on the south perennial cap has been identified by OMEGA [*Bibring et al.*, 2004] and CRISM [*Titus et al.*, 2008], confirming that the south perennial cap is presently a trap for water vapor.

[38] Similarly, the south seasonal CO_2 frost contains some fraction of water ice (from ~15 precipitable μm, [*Larson and Fink*, 1972] to hundreds of precipitable μm, [*Richardson and Wilson*, 2002; *Montmessin et al.*, 2004]) that is released into the atmosphere as the seasonal cap wanes. This water is transported pole-ward, back to the edge of the cap and cold trapped, following a process first described by *Houben et al.* [1997], modeled by *Montmessin et al.* [2004] and observed by *Kieffer and Titus* [2001], *Bibring et al.* [2005] and *Titus* [2005]. Ultimately, the water will be trapped on or at the edges of the perennial cap and may correspond to some of the exposed water ice mapped on Figure 3 and shown on Figures 3, 5, 6, 9, 10 and 11, forming a unit of transition between the perennial cap and the surrounding dusty surfaces.

[39] The regolith may act as a source of vapor during the spring, resulting in the spike of vapor in the atmosphere that was observed by TES [*Smith*, 2002, 2004] before Ls = 300°, when water ice is not yet exposed. In addition, the regolith may also act as a sink. The adsorption of H_2O molecules is controlled by the temperature and the water vapor partial pressure in the pore [*Jakosky*, 1985]. After Ls = 315–325°, as the surface and subsurface temperatures decrease, water vapor can be adsorbed back by the regolith [*Zent et al.*, 1986]. A fraction of the vapor originating from the exposed water ice may be adsorbed during the fall in the high latitude regolith.

[40] Finally, a fraction of the water vapor may remain in the atmosphere for longer periods of time and follow global winds. However, latitudinal vapor abundance during the southern spring indicates that little diffusion through the atmosphere occurs and that little H_2O is transported to latitudes lower than 40°S [*Smith*, 2002, 2004]. Conflicting results have been published regarding the net flux of H_2O of the south polar region. In the current Martian environment, there should be a net flux of water originating from the northern H_2O perennial cap, to the south polar region, due to the existence of the austral perennial CO_2 ice and the colder temperatures associated with it [*Jakosky*, 1983a, 1983b]. Over half an obliquity oscillation cycle (e.g., 5×10^4 years),

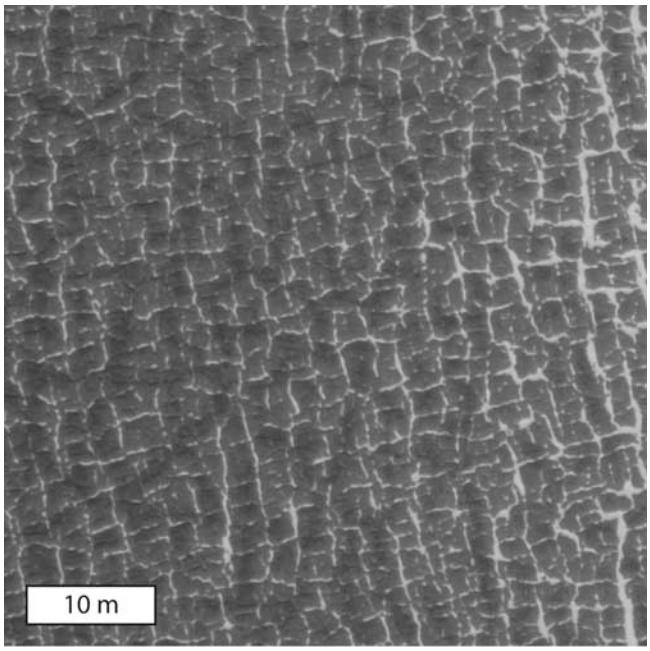

Figure 11. Meter-scale polygonal features outlined by residual CO_2 frost in the troughs, on exposed water ice. Polygonal landforms are expected to form at the high latitudes of Mars because of the stress induced by the contraction and expansion of the frozen regolith. PSP_005349_0930, 86.7°S, 111.1°E, Ls = 315°.

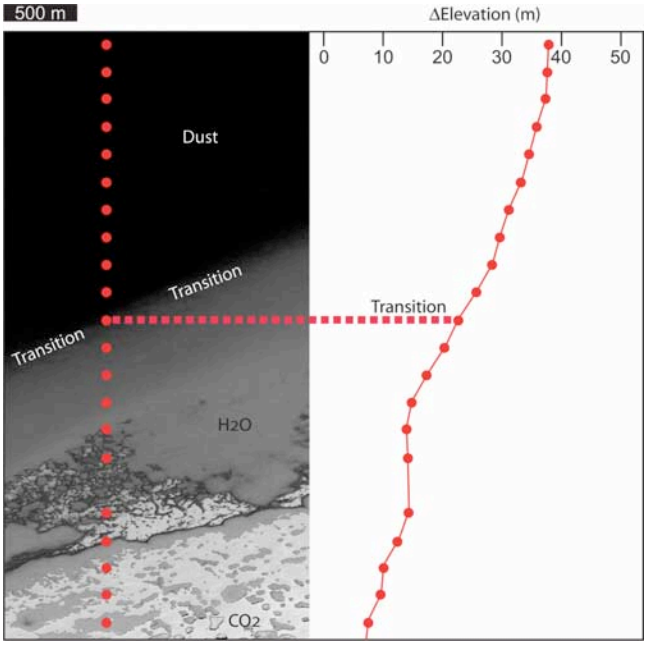

Figure 12. Example of regional slope determined with MOLA at the transition between exposed water ice and dust (M1500073, Ls = 345°, 83.9°S, 293.1°E). The red dots on the MOC image indicate the MOLA footprints acquired at the same time as M1500073. No jump of topography is detected at the contact between H_2O and dust suggesting that the thickness of the water ice sheet is not exceeding the detection limit for MOLA (i.e., a few meters at most).

15 m of ice may be lost by the north polar cap and gained by the south perennial cap and the SPLD [*Jakosky and Haberle*, 1992]. However, the details of the incorporation of H_2O ice in the SPLD is not known. At higher obliquity, the polar regions experience warmer summer seasons and perennial CO_2 caps are not likely to exist [*Toon et al.*, 1980]. Without an efficient cold trap at either of the poles, the amount of water vapor in the atmosphere rises significantly and is transported to the equatorial region and midlatitudes [*Jakosky and Carr*, 1985; *Mellon and Jakosky*, 1995; *Mellon et al.*, 1997]. At low obliquity, both poles are cooler than at present and accumulate water by cold-trapping atmospheric vapor. More recent general circulation models [*Richardson and Wilson*, 2002] suggest that for most orbital configurations, the south cap is experiencing a net loss of H_2O in favor of the north cap. *Fenton and Richardson* [2001] and *Richardson and Wilson* [2002] propose that the topographic dichotomy between the north and south hemispheres is responsible for a assymetrical Hadley circulation depleting the southern H_2O reservoir.

[41] Without re-deposition, the lifetime of the exposed water ice that is not on the CO_2 perennial cap is limited to short geologic periods because the sublimation rate likely corresponds to one of the highest erosive rates presently active on Mars. After Ls = 350°, the polar terrains are only a few K above the temperature of CO_2 frost and a fraction of the atmospheric water vapor will condense on the surface. Because exposed water ice surfaces are cooler than particulate surfaces at any time of the day before the polar night, H_2O vapor condenses preferentially on exposed water ice. The preferential condensation of vapor on exposed water ice at the end of the summer may compensate for part of the summer loss by sublimation, but it is not possible to quantify this flux because the vapor content of the atmosphere and other critical parameters are not known near the pole during the fall (see vapor retrieval technique limitations in the study by *Smith* [2002, 2004]).

[42] The presence of water ice adjacent to the south perennial cap is consistent with the hypothesis of the condensation of the atmospheric vapor originating from the north cap and high latitudes. The exposed water ice observed hundreds of kilometers away from the perennial CO_2 is not stable, and may be the relic of a thicker and wider H_2O ice sheet that formed 21,500 years ago as modeled by *Montmessin et al.* [2007]. It could also represent the relict of a former stable layer underlying portions of the perennial CO_2 cap [*Titus et al.*, 2003] that have been removed during a recent geologic time (e.g., centuries to millennia).

5. Conclusions

[43] We have mapped the distribution of carbon dioxide and exposed water ices near the south pole of Mars during the summer, when all of the seasonal CO_2 frost is removed, using THEMIS temperature measurements (Figure 3). Thermal mapping provides results in agreement with near infrared spectral data, and demonstrates that not only is water ice present, but that it must be the dominant phase in order to control the temperature.

[44] 1. Exposed water ice covers a surface area of ~40,000 km^2, mostly at the periphery of the perennial CO_2 cap, and on the mantled terrains adjacent to the SPLD. Most of the exposed water ice is not observed on the SPLD, which is the largest body of water ice on Mars, but at lower elevation, near 345°E and 83.5°S, where a 300 by 80 km continuous patch is entirely mapped for the first time.

[45] 2. Water ice on the CO_2 perennial cap is buffered at ~148 K and cannot be mapped with thermal data. OMEGA and CRISM observations are most suited for mapping H_2O ice on the CO_2 perennial cap.

[46] 3. At the meter to tens of meters scale, exposed water ice terrains are very uniform in term of roughness, albedo and surface features. The surface composition correlates extremely well with the albedo, which is remarkably homogeneous in the case of the exposed water ice (Figure 4) and has been calculated to be resulting from 8–80 μm ice crystals with 0.01 to 10% dust [*Titus et al.*, 2003] or 150 μm crystals with 30–35% dust [*Douté et al.*, 2007]. This suggests that the size of the H_2O crystals and the water-to-dust ratio are similar throughout the polar region.

[47] 4. When comparing the map of the distribution of the surface material (Figure 3) with Mariner 9 and Viking images, the present compositional and past albedo boundaries correlate extremely well. Assuming that the albedo/composition correlation observed today was also true in the recent past, we deduce that the distribution of the exposed water ice has been identical during the last four decades at the kilometer scale.

[48] 5. Because the retreat of the southern seasonal cap has followed the same pattern during the 20th century, and because it is strongly controlled by the occurrence of exposed water ice, it is likely that the distribution of exposed water ice has remained the same since at least the end of the 19th century.

[49] 6. Water ice surfaces accumulate more seasonal CO_2 frost during the fall and winter because they reach the carbon dioxide condensation temperature a few Martian days earlier ($\sim$10°Ls) than dusty surfaces. As a result, they are defrosted later in the summer, confirming that the CROCUS date is also partially controlled by the composition of the surface material (Figure 9).

[50] 7. The amount of vapor injected in the atmosphere by the sublimation of 40,000 km^2 of ice is not sufficient to account for the concentrations of vapor observed by TES during the southern summer. This confirms that other sources (e.g., regolith vapor diffusion, release of water trapped in the seasonal cap) are more important processes for the transfer of volatiles.

[51] 8. Exposed water ice is not stable in the current environment and sublimes at vertical rates ranging from a few tens to hundreds of microns per season. As a result, the lifetime of surface water ice is short, indicating that either re-deposition occurs (preferential condensation of atmospheric vapor on the cold exposed water ice surfaces in the late summer), that ice has been insulated from the atmosphere and uncovered recently (indicating the past location of the CO_2 residual cap), or that we are observing the remains of a larger water ice body deposited under other climate conditions and soon to be removed. Part of the current exposed water ice is also inherited from past and present cold-trapping of water vapor at the very edges and on the CO_2 perennial cap.

[52] 9. A specific morphology of polygonal landforms (<200 m in size, dark outlines, with width ranging from MOC sub-pixel resolution to $\sim$50 m, Figure 6) seems to be exclusively associated with exposed water ice (Figure 7). However, they only represent a small fraction of the ground patterns identified and mapped indicating that there is no general correlation between the distributions of ground patterns and exposed water ice (Figure 7).

[53] **Acknowledgments.** We would like to thank T. Titus for his comments on a preliminary version of this article, N. Bridges and N. Mangold for their helpful reviews. This work was supported by the NASA 2001 Mars Odyssey THEMIS Project.

References

Bandfield, J. L. (2007), High resolution subsurface water-ice distributions on Mars, *Nature*, *447*, 64–67, doi:10.1038/nature05781.

Bandfield, J. L., and W. C. Feldman (2008), Martian high latitude permafrost depth and surface cover thermal inertia distributions, *J. Geophys. Res.*, *113*, E08001, doi:10.1029/2007JE003007.

Bandfield, J. L., and M. D. Smith (2003), Multiple emission angle surface-atmosphere separations of thermal emission spectrometer data, *Icarus*, *161*, 47–65.

Bibring, J. P., et al. (2004), Perennial water ice identified in the south polar cap of Mars, *Science*, *428*, 627–630.

Bibring, J. P., et al. (2005), Mars surface diversity as revealed by the OMEGA/Mars Express observations, *Science*, *307*, 1576–1581.

Blasius, K. R., J. A. Cutts, and A. D. Howard (1982), Topography and stratigraphy of Martian layered deposits, *Icarus*, *50*, 4067–4091.

Boynton, W. V., et al. (2002), Distribution of hydrogen in the near surface of Mars: Evidence for subsurface ice deposits, *Science*, *297*, 81–85.

Byrne, S., and A. P. Ingersoll (2003), A sublimation model for Martian south polar ice features, *Science*, *299*, 1051–1053.

Christensen, P. R., et al. (2004), The Thermal Emission Imaging System (THEMIS) for the Mars 2001 Odyssey Mission, *Space Sci. Rev.*, *110*, 85–130.

Clifford, S. M., et al. (2000), The state and future of Mars polar science and exploration, *Icarus*, *144*, 210–242, doi:10.1006/icar.1999.6290.

Cutts, J. A. (1973), Nature and origin of layered deposits of the Martian polar regions, *J. Geophys. Res.*, *78*, 4231–4249.

Douté, S., B. Schmitt, Y. Langevin, J-P. Bibring, F. Altieri, G. Bellucci, B. Gondet, F. Poulet, and the MEX OMEGA team (2007), South pole of Mars: Nature and composition of the icy terrains from Mars Express OMEGA observations, *Planet. Space Rev.*, *55*, 113–133.

Fanale, F. P., and B. M. Jakosky (1982), Regolith-atmosphere exchange of water and carbon dioxide on Mars—Effects on atmospheric history and climate change, *Planet. Space Sci.*, *30*, 819–831.

Feldman, W. C., et al. (2004), Global distribution of near-surface hydrogen on Mars, *J. Geophys. Res.*, *109*, E09006, doi:10.1029/2003JE002160.

Fenton, L., and M. Richardson (2001), Martian surface winds: Insensitivity to orbital changes and implications for aeolian processes, *J. Geophys. Res.*, *106*(E12), 32,885–32,902.

Fergason, R. L., P. R. Christensen, and H. H. Kieffer (2006), High-resolution thermal inertia derived from the Thermal Emission Imaging System (THEMIS): Thermal model and applications, *J. Geophys. Res.*, *111*, E12004, doi:10.1029/2006JE002735.

Giauque, W. F., and J. W. Stout (1936), The entropy of water and third law of thermo-dynamics. The heat capacity of ice from 15 to 273 K, *J. Am. Chem. Soc.*, *58*, 1144.

Haberle, R. M., and B. M. Jakosky (1990), Sublimation and transport of water from the north residual polar cap on Mars, *J. Geophys. Res.*, *95*, 1423–1437.

Haberle, R. M., F. Forget, A. Colaprete, J. Schaeffer, W. V. Boynton, N. J. Kelly, and M. A. Chamberlain (2008), The effect of ground ice on the Martian seasonal CO_2 cycle, *Planet. Space. Sci.*, *56*, 251–255.

Herkenhoff, K. (2001), Geologic map of the MTM-85000 Quadrangle, Planum Australe Region of Mars, *U.S. Geol. Surv. Geol. Invest.*, *Map, I-2686*.

Herr, K. C., and G. C. Pimentel (1969), Infrared absorptions near three microns recorded over the polar caps of Mars, *Science*, *166*, 469–499.

Hobbs, P. V. (1974), *Ice Physics*, Clarendon Press, Oxford.

Houben, H. R., R. M. Haberle, R. E. Young, and A. P. Zent (1997), Modeling the Martian seasonal water cycle, *J. Geophys. Res.*, *102*(E4), 9069–9083.

Ingersoll, A. P. (1970), Mars: Occurrence of liquid water, *Icarus*, *168*, 972–973.

Ingersoll, A. P. (1974), The case against permanent CO_2 frost caps, *J. Geophys. Res.*, *79*, 3403–3410.

Jakosky, B. M. (1983a), The role of seasonal reservoirs in the Mars water cycle: I. Seasonal exchange of water with the regolith, *Icarus*, *55*, 1–18.

Jakosky, B. M. (1983b), The role of seasonal reservoirs in the Mars water cycle: II. Coupled models of the regolith, the polar caps, and atmospheric transport, *Icarus*, *55*, 19–39.

Jakosky, B. M. (1985), The seasonal cycle of water on Mars, *Space Sci. Rev.*, *41*, 131–200.

Jakosky, B. M., and M. H. Carr (1985), Possible precipitation of ice at low latitudes of Mars during periods of high obliquity, *Nature*, *315*, 559–561.

Jakosky, B. M., and C. B. Farmer (1982), The seasonal and global behavior of water vapor in the Mars atmosphere: Complete global results of the Viking atmospheric water detector experiment, *J. Geophys. Res.*, *87*(B4), 2999–3019.

Jakosky, B. M., and R. M. Haberle (1992), The seasonal behavior of water on Mars, in *Mars*, edited by H. H. Kieffer et al., pp. 969–1016, Univ. of Ariz. Press, Tucson, Ariz.

James, P. B., K. M. Malolepszy, and L. J. Martin (1987), Interannual variability of Mars' south polar cap, *Icarus*, *71*, 298–305.

Kieffer, H. H. (1970), Interpretation of the Martian polar cap spectra, *J. Geophys. Res.*, *75*, 510–514.

Kieffer, H. H. (1976), Martian north pole summer temperatures: Dirty water ice, *Science*, *194*, 1341–1344.

Kieffer, H. H. (1979), Mars south polar spring and summer temperatures: A residual CO_2 frost, *J. Geophys. Res.*, *84*, 8263–8288.

Kieffer, H. H. (2007), Cold jets in the Martian polar caps, *J. Geophys. Res.*, *112*, E08005, doi:10.1029/2006JE002816.

Kieffer, H. H., and T. N. Titus (2001), TES mapping of Mars's north polar cap, *Icarus*, *154*, 162–180.

Kieffer, H. H., S. C. Chase, E. Miner, G. Münch, and G. Neugebauer (1973), Preliminary report on infrared radiometric measurements from the Mariner 9 spacecraft, *J. Geophys. Res.*, *78*, 20,4291–4312.

Kieffer, H. H., T. N. Titus, K. F. Mullins, and P. R. Christensen (2000), Mars south polar spring and summer behavior observed by TES: Seasonal cap evolution controlled by frost grain size, *J. Geophys. Res.*, *105*(E4), 9653–9699.

Kieffer, H. H., P. R. Christensen, and T. N. Titus (2006), CO_2 jets formed by sublimation beneath translucent slab ice in Mars' seasonal polar ice cap, *Nature*, *442*, 793–796, doi:10.1038/nature04945.

Langevin, Y., S. Douté, M. Vincendon, F. Poulet, J.-P. Bibring, B. Gondet, B. Schmitt, and F. Forget (2006), No signature of clear CO_2 ice from the 'cryptic' regions in Mars' south seasonal polar cap, *Nature*, *442*, 790–792, doi:10.1038/nature05012.

Larson, H. P., and U. Fink (1972), Identification of carbon dioxide frost on the Martian polar caps, *Astrophys. J.*, *171*, L91–L95.

Lowell, P. (1896), *Mars*, Longmans and Green, London.

Malin, M. C., and K. S. Edgett (2001), Mars Global Surveyor Mars Orbiter Camera: Interplanetary cruise through primary mission, *J. Geophys. Res.*, *106*, 23,429–23,570.

Malin, M. C., M. A. Caplinger, and S. D. Davis (2001), Observational evidence for an active surface reservoir of solid carbon dioxide on Mars, *Science*, *294*, 2146–2148.

Mangold, N. (2005), High latitude patterned grounds on Mars: Classification, distribution and climatic control, *Icarus*, *174*, 336–359.

Mangold, N., S. Maurice, W. C. Feldman, F. Costard, and F. Forget (2004a), Spatial relationships between patterned ground and ground ice detected by the neutron spectrometer on Mars, *J. Geophys. Res.*, *109*, E08001, doi:10.1029/2004JE002235.

Mangold, N., F. Poulet, F. Forget, A. Gendrin, B. Gondet, Y. Langevin, B. Schmitt, J.-P. Bibring, and The OMEGA, Team (2004b), 35th COSPAR Scientific Assembly, 18–25 July 2004, Paris, France, p. 2700.

Marchant, D. R., A. R. Lewis, W. M. Phillips, E. J. Moore, R. A. Souchez, G. H. Denton, D. E. Sugden, N. Potter Jr., and G. P. Landis (2002), Formation of patterned ground and sublimation till over Miocene glacier ice in Beacon Valley, southern Victoria Land, Antarctica, *Geol. Soc. Am. Bull.*, *114*, 6,718–730, doi:10.1130/0016-7606.

Mellon, M. T. (1997), Small-scale polygonal features on Mars: Seasonal thermal contraction cracks in permafrost, *J. Geophys. Res.*, *102*(E11), 25,617–25,628.

Mellon, M. T., and B. M. Jakosky (1995), The distribution and behavior of Martian ground ice during past and present epochs, *J. Geophys. Res.*, *100*(E6), 11,781–11,799.

Mellon, M. T., B. M. Jakosky, and S. E. Postawko (1997), The persistence of equatorial ground ice on Mars, *J. Geophys. Res.*, *102*(E8), 19,357–19,369.

Mellon, M. T., W. C. Feldman, and T. H. Prettyman (2004), The presence and stability of ground ice in the southern hemisphere of Mars, *Icarus*, *169*, 324–340.

Milkovich, S. M., and J. W. Head III (2005), North polar cap of Mars: Polar layered deposit characterization and identification of a fundamental climate signal, *J. Geophys. Res.*, *110*, E01005, doi:10.1029/2004JE002349.

Mitrofanov, I., et al. (2002), Maps of subsurface hydrogen from the high energy neutron detector, Mars Odyssey, *Science*, *297*, 5578, 78–81, doi:10.1126/science.1073616.

Montmessin, F., F. Forget, P. Rannou, M. Cabane, and R. M. Haberle (2004), Origin and role of water ice clouds in the Martian water cycle as inferred from a general circulation model, *J. Geophys. Res.*, *109*, E10004, doi:10.1029/2004JE002284.

Montmessin, F., H. B. Haberle, F. Forget, Y. Langevin, R. T. Clancy, and J.-P. Bibring (2007), On the origin of perennial water ice at the south pole of Mars: A precession controlled mechanism?, *J. Geophys. Res.*, *112*, E08S17, doi:10.1029/2007JE002902.

Murray, B. C., L. A. Soderblom, J. A. Cutts, R. P. Sharps, D. J. Milton, and R. B. Leighton (1972), Geological framework of the south polar region of Mars, *Icarus*, *17*, 328–345.

Nye, J. F., W. B. Durham, P. M. Schenk, and J. M. Moore (2000), The instability of a south polar cap on Mars composed of carbon dioxide, *Icarus*, *144*, 449–455, doi:10.1006/icar.1999.6306.

Pimentel, G. C., P. B. Forney, and K. C. Herr (1974), Evidence about hydrate and solid water in the Martian surface from the 1969 Mariner infrared spectrometer, *J. Geophys. Res.*, *79*, 1623–1634.

Piqueux, S., and P. R. Christensen (2008a), Deposition of CO_2 and erosion of the Martian south perennial cap between 1972 and 2004: Implications for current climate change, *J. Geophys. Res.*, *113*, E02006, doi:10.1029/2007JE002969.

Piqueux, S., and P. R. Christensen (2008b), North and south sub ice gas flow and venting of the seasonal caps of Mars: A major geomorphological agent, *J. Geophys. Res.*, *113*, E06005, doi:10.1029/2007JE003009.

Piqueux, S., S. Byrne, and M. I. Richardson (2003), Sublimation of Mars' southern seasonal CO_2 cap and the formation of spiders, *J. Geophys. Res.*, *108*(E8), 5084, doi:10.1029/2002JE002007.

Plaut, J. J., et al. (2007), Subsurface radar sounding of the south polar layered deposits of Mars, *Science*, *316*, 5821, 92–95, doi:10.1126/science.1139672.

Presley, M. A., and P. R. Christensen (1997), Thermal conductivity measurements of particulate materials: 2. Results, *J. Geophys. Res.*, *102*(E3), 6551–6566, doi:10.1029/96JE03303.

Putzig, N. E., and M. T. Mellon (2007a), Apparent thermal inertia and the surface heterogeneity of Mars, *Icarus*, *191*, 68–94, doi:10.1016/j.icarus.2007.05.013.

Putzig, N. E., and M. T. Mellon (2007b), thermal behavior of horizontally mixed surfaces on Mars, *Icarus*, *191*, 52–67, doi:10.1016/j.icarus.2007.03.022.

Richardson, M. I., and R. J. Wilson (2002), A topographically forced asymmetry in the Martian circulation and climate, *Nature*, *416*, 298–401, doi:10.1038/416298a.

Smith, M. D. (2002), The annual cycle of water vapor on Mars as observed by the thermal emission spectrometer, *J. Geophys. Res.*, *107*(E11), 5115, doi:10.1029/2001JE001522.

Smith, M. D. (2004), Interannual variability in TES atmospheric observations of Mars during 1999–2003, *Icarus*, *167*, 148–165, doi:10.1016/j.icarus.2003.09.010.

Smith, D. E., et al. (1999), The global topography of Mars and implications for surface evolution, *Science*, *284*, 5419, 1495–1503, doi:10.1126/science.284.5419.1495.

Smith, D. E., M. T. Zuber, and G. A. Neumann (2001), Seasonal variations of snow depth on Mars, *Science*, *294*, 2141–2146.

Smith, M. D., J. L. Bandfield, M. I. Richardson, P. R. Christensen (2002), Recent atmospheric observations of Mars by THEMIS and TES, presented at the annual meeting of the Division of Planetary Science, Birmingham, AL, 6–11 October.

Soderblom, L. A., M. C. Malin, J. A. Cutts, and B. C. Murray (1973), Mariner 9 observations of the surface of Mars in the north polar region, *J. Geophys. Res.*, *78*, 4197–4210.

Thomas, P. C., M. C. Malin, K. S. Edgett, M. H. Carr, W. K. Hartmann, A. P. Ingersoll, P. B. James, L. A. Soderblom, J. Veverka, and R. Sullivan (2000), North-south geological differences between the residual polar caps on Mars, *Nature*, *404*, 161–164.

Thomas, P. C., M. C. Malin, P. B. James, B. A. Cantor, R. M. E. Williams, and P. Gierasch (2005), South polar residual cap of Mars: Features, stratigraphy, and changes, *Icarus*, *174*, 535–559.

Titus, T. N. (2005), Thermal infrared and visual observations of a water ice lag in the Mars southern summer, *Geophys. Res. Lett.*, *32*, L24204, doi:10.1029/2005GL024211.

Titus, N. T., H. H. Kieffer, and P. R. Christensen (2003), Exposed water ice discovered near the South pole of Mars, *Science*, *299*, 1048–1051.

Titus, T. N., et al. (2004), Intra-annual variations of the Martian Swiss Cheese terrain (abstract), *35th Lunar Planet. Sci. Conf.*, League City, TX, 2005.

Titus, T. N., A. Brown, F. P. Seelos, S. L. Murchie, S. Piqueux, P. R. Christensen, and The CRISM Team (2008), Infrared observations of Mars south polar residual cap: When eating Swiss Cheese—Use a fork (abstract), *Lunar Planet. Sci. Conf.*, 2359.

Toigo, A. D., M. I. Richardson, R. J. Wilson, H. Wang, and A. P. Ingersoll (2002), A first look at dust lifting and dust storms near the south pole of Mars with a mesoscale model, *J. Geophys. Res.*, *107*(E7), 5050, doi:10.1029/2001JE001592.

Toon, O. B., J. B. Pollack, W. Ward, J. A. Burns, and K. Bilski (1980), The astronomical theory of climatic change on Mars, *Icarus*, *44*, 552–607.

van Gasselt, S., D. Reiss, A. K. Thorpe, and G. Neukum (2005), Seasonal variations of polygonal thermal contraction cracks patterns in a south polar trough, Mars, *J. Geophys. Res.*, *110*, E08002, doi:10.1029/2004JE002385.

Winfree, K. N., and T. N. Titus (2007), Trends in the south polar cap of Mars, #3373, paper presented at *7th Int. Conf. Mars*, Pasadena, Calif.

Zent, A. P., F. P. Fanale, J. R. Salvail, and S. E. Postawko (1986), Distribution and state of H_2O in the high-latitude shallow sub-surface of Mars, *Icarus*, *67*, 19–36.

Zuber, M. T., et al. (2007a), Density of Mars' south polar layered deposits, *Science*, *317*, 5845, 1718–1719, doi:10.1126/science.1146995.

Zuber, M. T., F. G. Lemoine, D. E. Smith, A. S. Konopliv, S. E. Smrekar, and S. W. Asmar (2007b), Mars Reconnaissance Orbiter Radio Science Gravity Investigation, *J. Geophys. Res.*, *112*, E05S07, doi:10.1029/2006JE002833.

P. R. Christensen, C. S. Edwards, and S. Piqueux, School of Earth and Space Exploration, Arizona State University, Tempe, AZ 85287, USA. (phil.christensen@asu.edu; christopher.edwards@asu.edu; sylvain.piqueux@asu.edu)